JOURNAL OF MATERIALS SCIENCE 17 (1982) 732–740

The nature of acicular ferrite in HSLA steel weld metals

R. A. RICKS, P. R. HOWELL G. S. BARRITTE
Department of Metallurgy and Materials Science, University of Cambridge, Pembroke Street, Cambridge, UK

In this paper, the nature of the fine interlocking acicular ferrite microstructure in HSLA steel weld metals is investigated. The results strongly suggest the acicular ferrite is comprised of intragranularly nucleated Widmanstätten ferrite. Further, it is shown that the active nucleation sites for this ferritic product are weld metal inclusions. Sympathetic nucleation then takes place which leads eventually to the fine, interlocking microstructure which is a characteristic of acicular ferrite.

1. Introduction

High-strength low-alloy (HSLA) steels are extensively used in welded engineering components and a considerable number of investigations have been directed at optimizing structure–property relationships in such welds (see, for example, [1–4]. Of particular importance is the development of the fine microstructural constituent which has been termed "acicular ferrite" since it is known to enhance both the toughness and strength of welds [1].

The development of ferritic microstructures in conventionally-wrought steels has been extensively studied (see, for example, [5]) and the microstructures charaterised by Dubé and co-workers [6, 7]. However, the development of ferritic microstructure in weld metals has received somewhat less attention and some controversy still exists concerning the nature and terminology of the ferritic reaction products.

In this paper, one particular reaction product in HSLA steel weld metals is examined, namely acicular ferrite. Specifically, the morphology and development of this intragranularly nucleated phase are examined, and the role of inclusions in the nucleation of acicular ferrite is discussed. In addition, the effect of the inclusions on the weld metal chemistry is considered.

2. Experimental procedure

Weld beads were obtained by depositing a manual metal arc weld onto a clean steel plate using a metal electrode coated with a basic flux. Details of the welding conditions and the compositions of both weld deposit and base-plate are given in Tables I and II, respectively. The welded plate was either air cooled or ice-brine quenched immediately after the welding process was completed. Air cooling the weldment produced a fully transformed microstructure whilst quenching led to a partially transformed structure.*

Specimens for microstructural examination were slit from the weld deposits under conditions of flood lubrication. For light optical microscopy, specimens were mechanically-polished using diamond lapping compounds to 0.25 μm prior to etching in 2 vol% nital. Carbon extraction replicas

TABLE I Welding conditions

Weld type	Bead on plate (12 mm)
Voltage	23 V
Current	215 A
Electrode travel speed	170 mm min^{-1}
Heat input	1.75 kJ mm^{-1}
Electrode type	E.S.A.B. "Tensitrode 55" (Basic low-hydrogen electrode with Fe powder additions to coating (type E7018))

*The term "fully transformed" describes the situation whereby the decomposition of austenite has led to a ferrite–pearlite microstructure. In contrast, "partial transformation" relates to the instance where the ferrite–pearlite reaction has been interupted by the quench, the remaining austenite being wholly or fully transformed to bainite or martensite.

0022–2461/82/030732–09$03.58/0

TABLE II Bulk composition of base-plate and weld metal

Material	Composition (wt%)										
	C	Si	Mn	S	P	O_2	N_2	Al	Ti	V	Nb
Base-plate	0.15	0.32	1.02	0.025	0.011	0.003	0.003	0.04	< 0.01	< 0.01	< 0.005
Weld metal	0.09	0.51	1.42	0.012	0.013	0.021	0.007	0.015	0.011	< 0.01	< 0.005

were obtained from the light optical specimens, the replicas being removed from the specimen by electro-etching in a 5% nital solution. Thin-foil transmission electron microscope specimens were prepared from 3 mm diameter discs of the weld metal. The discs were mechanically ground to 0.1 mm thickness and thinned in a twin-jet electropolisher using an electrolyte consisting of 5 vol% perchloric acid and 95 vol% glacial acetic acid at room temperature and at a potential of 90 V.

Electron microscopy was performed on a Phillips EM 300 and an EM 400 TEM/STEM equipped with an energy dispersive X-ray spectrometer. The compositions of various features of the weld metal microstructure were determined from the X-ray spectra using a Link systems 860 analyser employing standard commercial thin-foil correction programmes.

3. Results

3.1. The nature of acicular ferrite

The fully transformed microstructure of the weld is shown in Fig. 1. Proeutectoid ferrite has formed on the prior-austenite grain boundaries (arrowed in Fig. 1a) whilst the interior of the austenite grains comprise the fine interlocking constituent which has been termed acicular ferrite (Fig. 1b). It should be noted that this constituent is formed in the body of the austenite grains. It is not a sectioning effect produced by primary side plates originating from austenite grain boundaries above or below the plane of polish. This may be gauged by comparing the scale of the acicular ferrite units with that of the austenite grain size. Fig. 2 shows the partially transformed microstructure produced by iced-brine quenching. Again pro-eutectoid ferrite has formed on the austenite grain boundaries (arrowed), whilst the interior of the austenite grains is now seen to contain some isolated intragranular Widmanstätten ferrite plates (e.g., at at A in Fig. 1b) in a bainitic–martensitic matrix, which was formed during the quench.

Transmission electron microscopy of thin-foil specimens showed that the acicular ferrite constituent consisted of fine ferrite laths or plates, as is shown in Fig. 3a and b. In both instances, it can be seen that individual laths contain a relatively high dislocation density and some recovery of the dislocation sub-structure has occured (e.g. at A and B in Fig. 3a and b, respectively). Examination of the partially transformed welds revealed the presence of both retained austenite (Fig. 4a) and

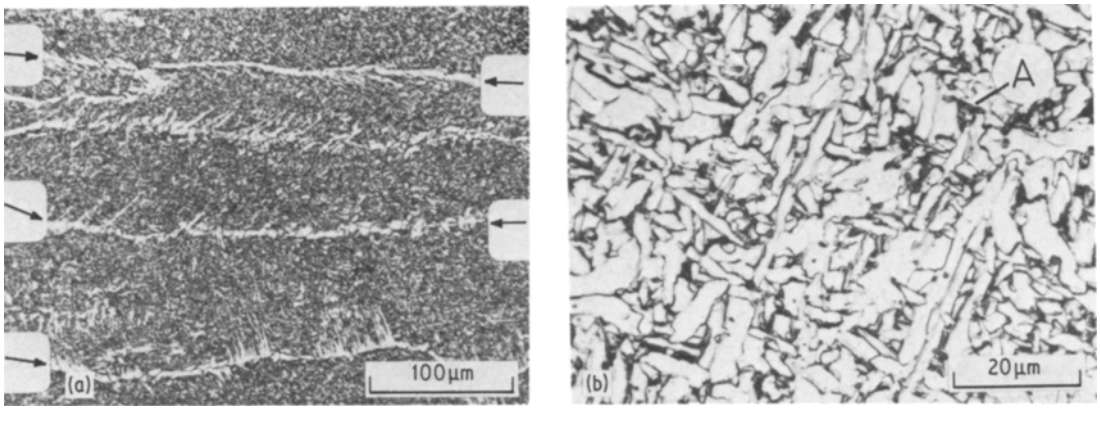

Figure 1 Light optical micrographs of the fully transformed manual metal arc weld. (a) low-magnification image showing the development of pro-eutectoid ferrite at the prior austenite grain boundaries. The body of the prior austenite grains comprise the acicular ferrite constituent; (b) higher magnification image illustrating the interlocked nature of the acicular ferrite microstructure. The dark etching areas (for example, at A) correspond to regions of either austenite, martensite or pearlite.

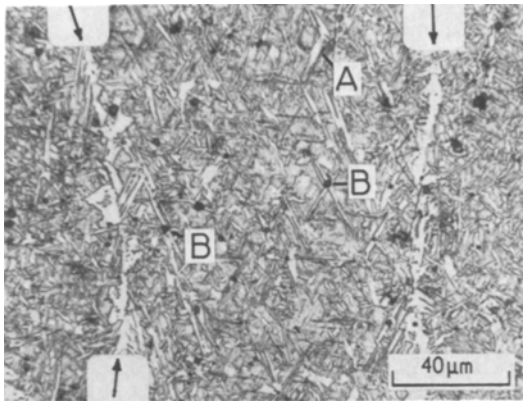

Figure 2 Light optical micrograph of the partially transformed weld metal. Pro-eutectoid ferrite has formed on the austenite grain boundaries (arrowed). Nucleation of intragranular Widmanstätten ferrite has also occurred (for example, at A) and a close association between this ferrite and the weld-metal inclusions is often observed (for example, at B).

twinned martensite (Fig. 4b and c). These observations suggest that during the growth of acicular ferrite, significant carbon enrichment of the untransformed austenite occurs such that, on quenching, this austenite is retained or is transformed to high carbon, or twinned, martensite. Further evidence for the carbon enrichment of the untransformed austenite was provided by the observation of ferrite–carbide aggregate regions in the fully transformed microstructure. Fig. 5a and b shows examples of these aggregate regions, which closely resemble the morphology of degenerate pearlite found in a number of isothermally-transformed steels [8, 9].

These results indicate that the formation of acicular ferrite is associated with a carbon partitioning reaction and is therefore a pro-eutectoid phase. Further, it is suggested that the individual ferrite units are intragranularly nucleated Widmanstätten ferrite, since no carbide precipitation is observed either at the lath boundaries, or within the laths themselves (see Fig. 3a and b) as would be expected if the transformation were bainitic in character.

In addition, stepped-growth interfaces were frequently observed between the acicular ferrite and the austenite or martensite regions, as shown in Fig. 4a and c (arrowed). These results imply that a ledge mechanism [10] is operative during the formation of acicular ferrite in a manner analogous to that documented for the lateral growth of austenite grain-boundary nucleated Widmanstätten ferrite [11, 12].

3.2. The nucleation of acicular ferrite

Reference to Fig. 2 shows that many of the intragranularly-nucleated Widmanstätten ferrite plates are associated with weld-metal inclusions (e.g., at B in Fig. 2). This association was confirmed using transmission electron microscopy of both carbon extration replicas and thin-foil specimens. Fig. 6a and b is taken from carbon extraction replicas of the partially transformed weld. In both instances, it can be seen that single large intragranular plates (A) are intimately associated with inclusions (arrowed). In many instances, however, it was found that multiple ferrite nucleation occured at inclusions. Fig. 7a and b shows thin-foil micrographs illustrating this point. In Fig. 7a, a single inclusion has nucleated plates A, B, and C

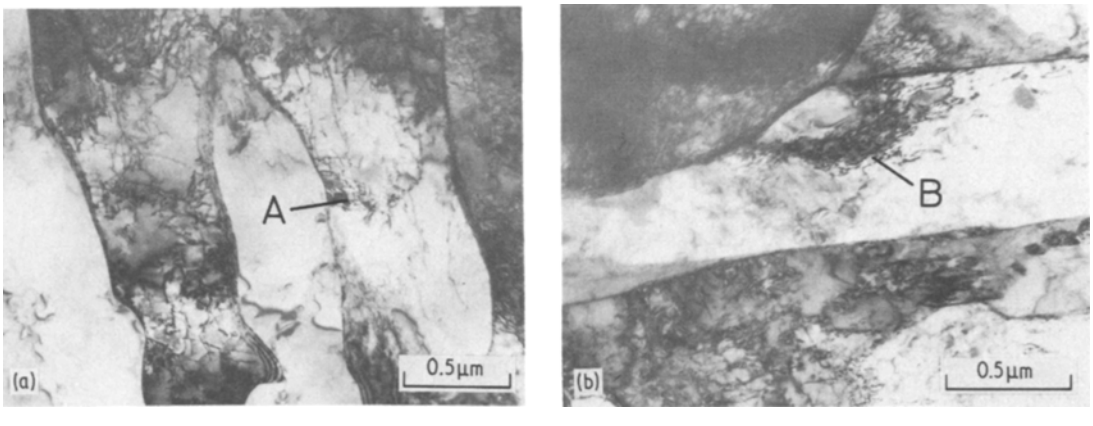

Figure 3 Transmission electron micrographs of the acicular ferrite constituent illustrating the relatively high dislocation density with individual laths/plates. There is also some tendency towards recovery of the defect structure (for example, at A and B).

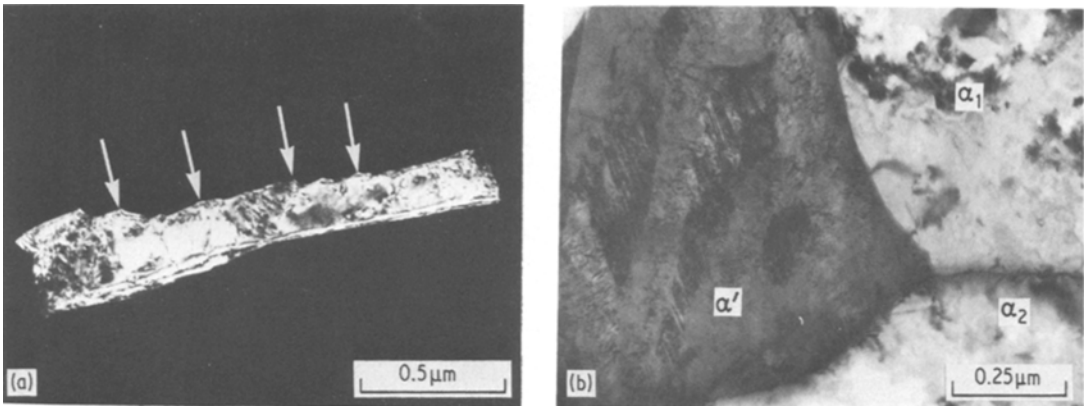

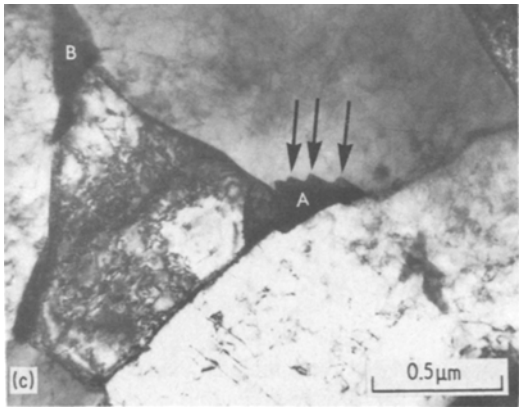

Figure 4 Transmission electron micrographs of retained austenite and twinned martensite in partially transformed specimen material. (a) Centred dark-filed micrograph of retained austenite. One of the acicular ferrite–austenite interfaces is ledged, the steps being arrowed. (b) Internally-twinned martensite (α') and two acicular ferrite grains (α_1 and α_2). In this instance, both interfaces appear to be smoothly curved. (c) Two martensite islands (at A and B). The interface between the martensite island at A and the upper acicular ferrite grain contains a number of steps (arrowed).

whilst in Fig. 7b, four Widmanstätten plates (A to D) are seen to radiate from two closely-spaced inclusions. This latter image closely resembles the "Widmanstätten Star", as discussed by Aaronson and Wells [13].

In addition to the nucleation of intragranular ferrite on inclusions, it was found that ferrite side-plates could develop from pre-existing inclusion-nucleated Widmanstätten ferrite (i.e., ferrite could be sympathetically nucleated [13]). For example, Fig. 6a shows a number of sympathetic nucleation events* (e.g., at B, C and D), whilst Fig. 8 illustrates the complex interlocking ferrite network that can result from multiple sympathetic nucleation. Hence, it would appear that sympathetic nucleation can play an dominant role in the development of the acicular ferrite microstructure. Sympathetic nucleation at grain-boundary allotriomorphs and side-plates may also occur, but, in view of the large austenite grain-size present in these alloys, nucleation on intragranular inclusions must represent the vital initial stage in the formation of acicular ferrite. It should be appreciated that homogeneous nuclation of ferrite is highly unlikely (see Section 4) owing to the high energy barrier associated with this type of nucleation.

4. Discussion

The results of the previous section have shown that the acicular ferrite constituent of weld metal microstructures is comprised of intragranularly-nucleated Widmanstätten ferrite and that the primary nucleation sites are refractory inclusions. The fine interlocking microstructure which is characteristic of acicular ferrite may then be related to subsequent multiple sympathetic nucleation events.

Inclusions promote the intragranular nucleation of ferrite in three ways:

(a) by acting as a substrate such that the destruction of part of the austenite–inclusion interface by the formation of a ferrite nucleus reduces the overall energy barrier to nucleation;

(b) by the product phase nucleus (i. e., ferrite) adopting rational orientation relationships with respect to both the inclusion and the austenite

*It should be noted that the primary side-plate and the associated secondary plates are not of the same orientation since they are separated by well-defined grain boundaries.

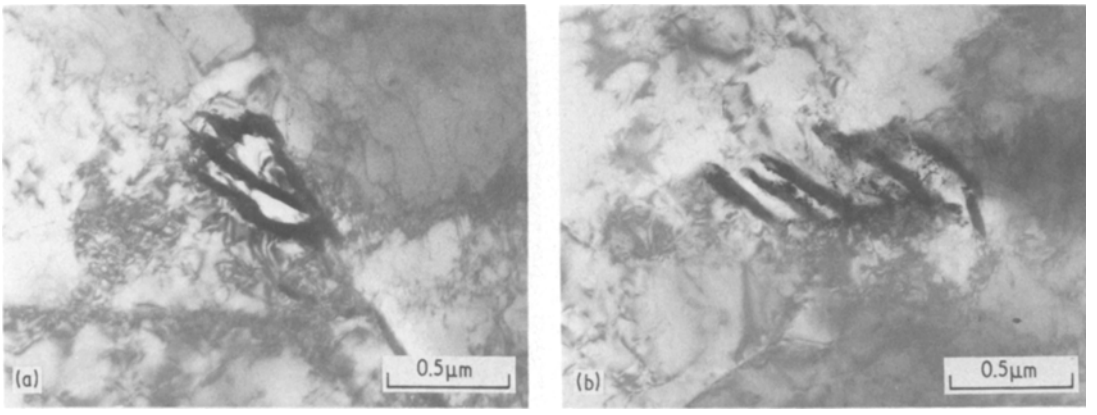

Figure 5 Transmission electron micrographs of ferrite–carbide aggregates which form towards the end of the transformation.

such that low-energy interfaces may form between the nuleus and both the austenite and inclusion; and

(c) by affecting the local chemistry of the austenite such that the driving force for the transformation may be increased.

The efficiency of inclusions as substrates for nucleation has been examined recently [14] using classical nucleation theory (e.g., [15, 16]). In this treatment the inclusions were considered to be inert, incoherent and non-deformable. The major findings of this investigation are shown in Fig. 9 and can be summarised as follows:

(1) Irrespective of inclusion size, inclusion nucleation is always energetically less favourable than nucleation at austenite grain boundaries for a given driving force; and

(2) Nucleation at inclusions is always more favourable than homogeneous nucleation at constant driving force.

Inclusion nucleation will be promoted further if the ferrite can adopt a rational orientation relationship with both the austenite and inclusion [16]. In view of the nature of the inclusions present, this would appear to be highly unlikely. The same is also true if any VN or TiN particles are present in the austenite, since the ferrite would have to be related as described by Baker and Nutting [17] to the nitride and as described by Kurdjumov and Sachs [18] to the austenite: a situation which can not hold if the nitrides are cube–cube related to the austenite [14]. The above considerations imply that, at high transformation temperatures, nucleation at austenite grain boundaries will predominate since the relatively low driving force for austenite decomposition will inhibit inclusion nucleation events occurring. Hence, under conditions of continuous cooling (i.e., the situation pertaining to the decomposition of austenite in

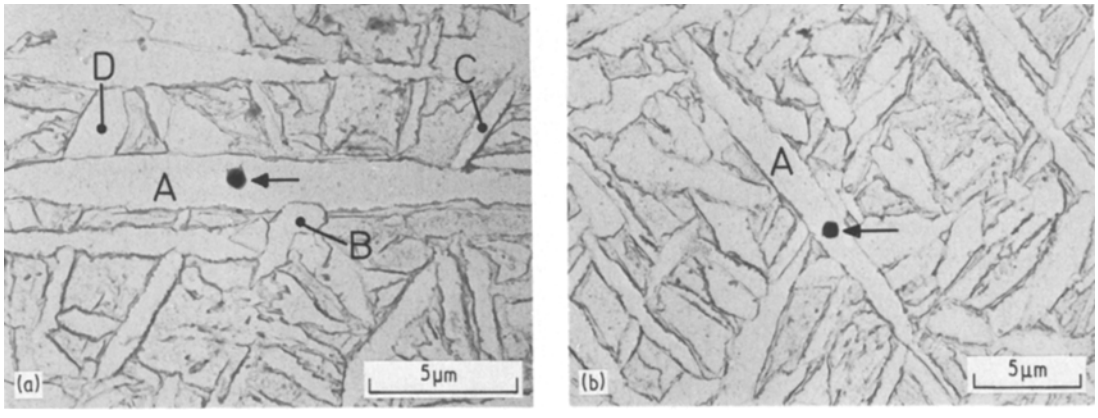

Figure 6 Transmission electron micrographs (of a carbon electron extration replica) from partially-transformed specimen material. (a) nucleation of intragranular Widmanstätten ferrite (A) at an inclusion (arrowed). Evidence for the sympathetic nucleation of ferrite is also observed (e.g., at B, C and D). (b) The same as (a) but a large Widmanstätten plate (A) has nucleated at an inclusion (arrowed).

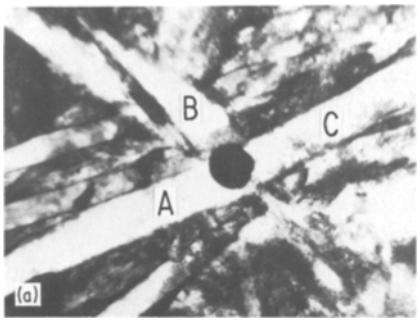

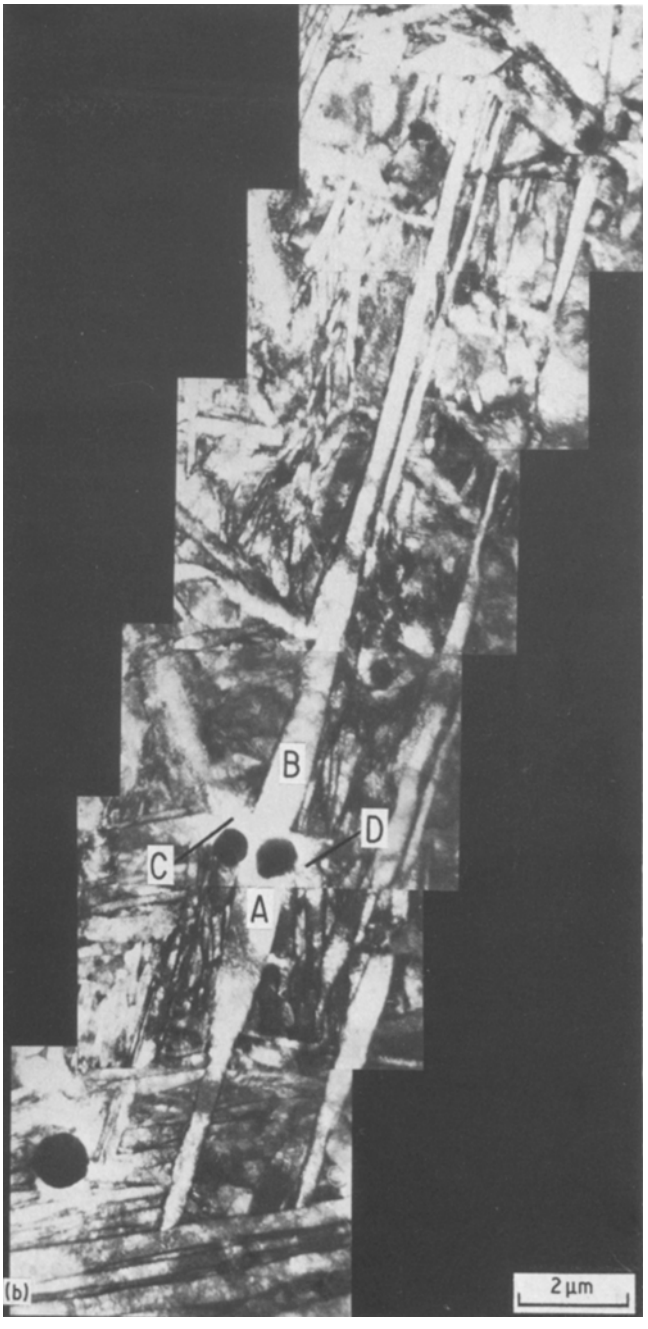

Figure 7 Transmission electron micrographs illustrating multiple nucleation. (a) Three Widmanstätten plates (at A, B and C) in association with an inclusion. The matrix is lath martensite. (b) Multiple nucleation of Widmanstätten ferrite at two closely-spaced inclusions.

weld metals) austenite grain-boundary nucleation should always occur at higher temperatures than inclusion nucleation. This point is illustrated in Fig. 2 where the grain-boundary nucleated ferrite is considerably coarser than the intragranularly nucleated ferrite. Similary, if the quench is sufficiently rapid after welding is completed, it is possible to wholly suppress any intergranular nucleation whilst maintaining almost continuous films of grain-boundary ferrite. Thus, site saturation at the austenite grain boundaries invariably precedes the onset of inclusion nucleation.

The weld-metal inclusions have been examined using energy dispersive spectrometry (EDS) to determine their chemistry [19]. Fig. 10a and b shows typical X-ray spectra from a weld-metal inclusion. The major peaks present are characteristic of Al, Si, S, Ti and Mn, which suggests

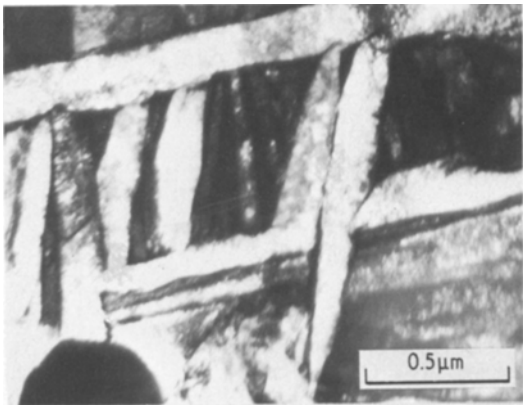

Figure 8 An example of the complex interlocking ferrite network that can arise from multiple sympathetic nucleation. The darker areas in this micrograph are lath martensite.

that the inclusions most probably comprise mixed Al and Mn silicates, Al and Ti oxides and manganese sulphide. Hence, it might be expected that both the Mn- and Si-levels in the adjacent austenite would be lower than in that well-removed from the inclusions; This in turn could lead to a change in the driving force for ferrite nucleation at the inclusion. However, the application of STEM (scanning transmission electron microscopy)/EDS techniques has shown that no detectable variations in either Mn- or Si-levels are present [19]. This is illustrated in Fig. 11a and b which shows the Mn and Si concentration profiles up to an inclusion (located at the origin). Hence, it would appear that the major effect that the inclusions exert on the ferrite is to lower the energy barrier to nucleation by decreasing the surface area of interphase boundaries formed by nucleation.

Finally, it should be noted that the grain-boundary ferrite reaction and the intragranular ferrite reaction are competitive. In the weld metal investigated here, the acicular ferrite reaction predominates; however, in other HSLA weld metals the microstructure can be comprised almost exclusively of grain-boundary nucleated ferrite. The relative proportion of the two transformation products obtained in any one system is a function of a number of parameters, including the austenite grain-size, cooling rate, inclusion distribution and weld-metal chemistry (see for example, [14]).

4. Summary

The results detailed in the previous sections have shown that:

(a) acicular ferrite is comprised of intragranularly-nucleated Widmanstätten ferrite, as suggested by Abson and Dolby [20] and Cochrane and Kirkwood [21],

(b) intragranular nucleation of ferrite occurs at lower transformation temperatures than that characteristic of austenite grain-boundary nucleation and after site saturation has occured at the boundaries;

(c) the nucleation and growth of acicular ferrite continues until the remaining austenite is sufficiently enriched in carbon to decompose to a ferrite–carbide aggregate which is similar in nature to degenerate pearlite;

(d) weld-metal inclusions are the primary nucleation sites for intragranular Widmanstätten

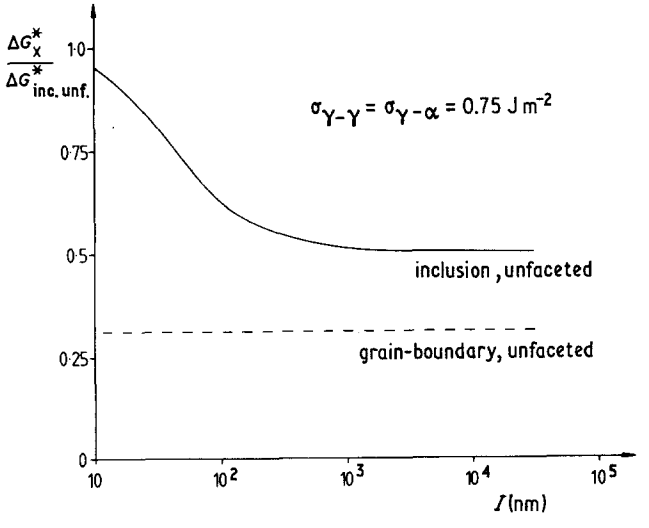

Figure 9 Variation in the energy barrier to nucleation, ΔG_x, normalized to that corresponding to unfaceted homogeneous nucleation in an austenite matrix, for unfaceted ferrite formed on an inclusion ($\Delta G^*_{inc.unf.}$), as a function of inclusion radius, *l*. Constant values of the volume free-energy change ($\Delta G_v = -300\ J\ mol^{-1}$) and surface free-energy of both austenite–austenite and austenite–ferrite boundaries ($\sigma = 0.75\ J\ m^{-2}$) are assumed. The equivalent energy barrier for austenite grain-boundary nucleation is also shown ($\Delta G^*_{g.b.unf.}$).

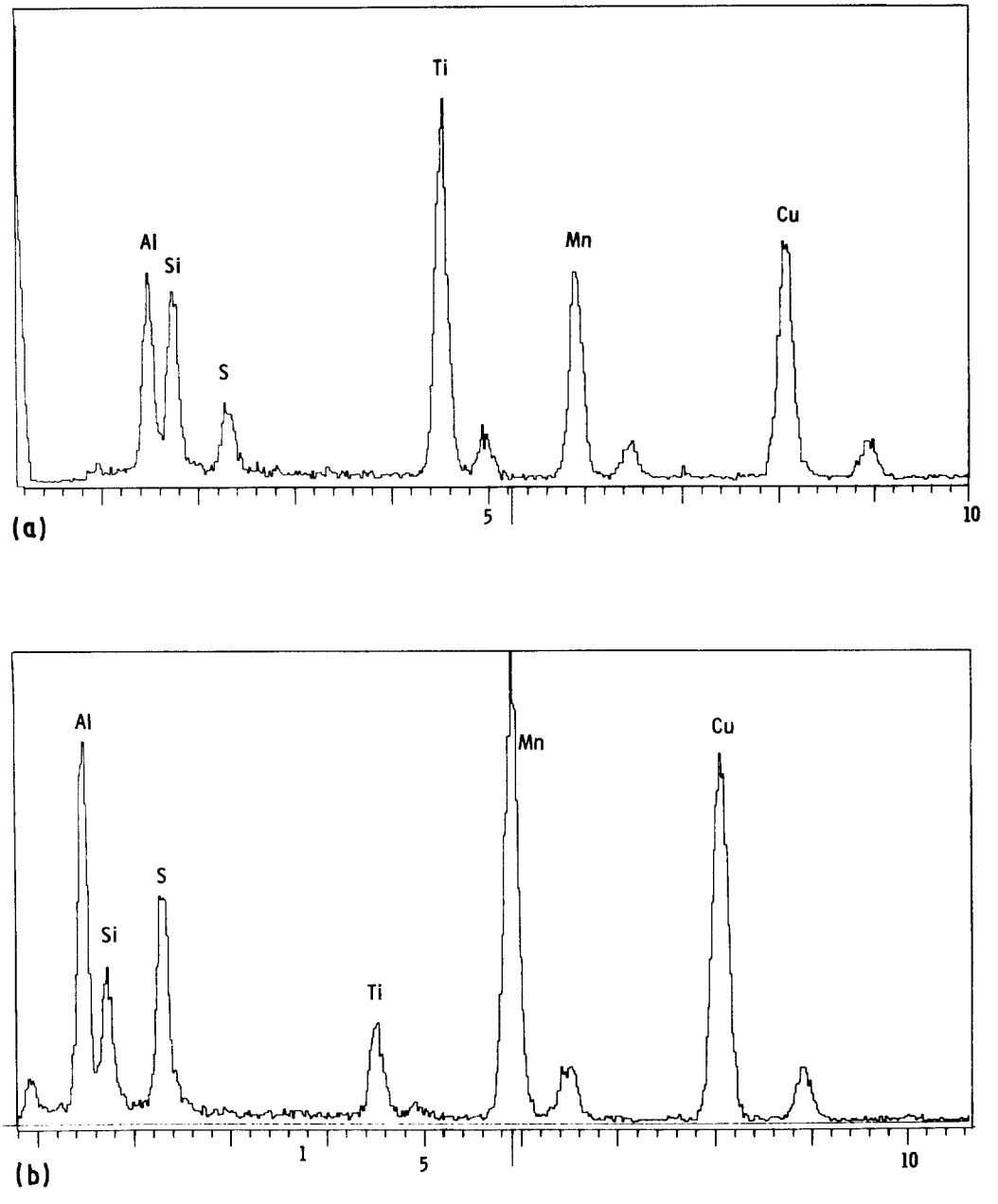

Figure 10 Typical X-ray spectra from a single inclusion using a 10 nm probe. (a) Spectra from the centre of the inclusion. The major peaks present are Al, Si, S, Ti and Mn. The Cu-peak arises from the support grid and is not characteristic of the inclusion. (b) Spectra from the edge of the same inclusion. Although the same peaks are still present, their relative magnitudes have changed. From these and other similar spectra, it is suggested that the periphery of the inclusion is rich in manganese sulphide.

ferrite, as proposed by Abson and Dolby [18];

(e) the major effect of weld-metal inclusions in the nucleation of ferrite is through their ability to reduce the energy barrier to nucleation by acting as an inert substrate; and

(f) sympathetic nucleation of ferrite occurs and this leads to the fine interlocked nature of acicular ferrite.

Acknowledgements

The authors are grateful to Professor R. W. K. Honeycombe, FRS, for the provision of laboratory

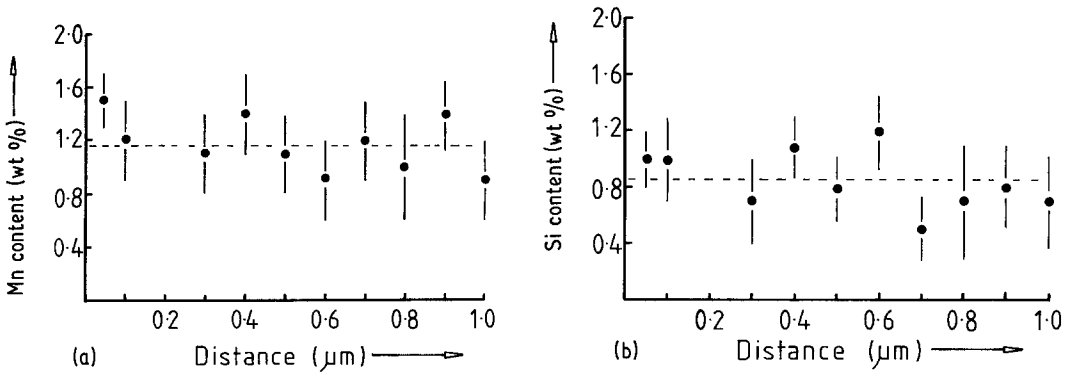

Figure 11 STEM composition profiles up to an inclusion (located at the origin). (a) Mn-profile, no detectable variation in Mn-level is observed. (b) Si-profile, again, no systematic change in Si-level is detected.

facilities and for his continued interest and encouragement. Financial support was received from the SRC and the Welding Institute and is gratefully acknowledged. The Welding Institute is also thanked for preparing the weld deposits.

References

1. R. E. DOLBY, "Factors Controlling Weld Toughness – the present Position, Part II – Weld Metals" Welding Institute Research Report No. 14/1976/M (Welding Institute, London, 1976).
2. Y. ITO and M. NAKANISHI, "Study on Charpy Impact Properties of Weld Metal with Submerged Arc Welding" The Sutitomo Search, No. 15, (1976) p. 42.
3. J. G. GARLAND and P. R. KIRKWOOD, *Metal Constr.* (1975) 275.
4. *Idem, ibid.* (1975) 320.
5. E. LEVINE and D. C. HILL, *ibid.* (1977) 346.
6. E. S. DAVENPORT and E. C. BAIN, *Trans A. I. M. E.* **90** (1930) 117.
7. C. A. DUBÉ, H. I. AARONSON and R. F. MEHL, *Rev. Met.* **55** (1958) 201.
8. H. I. AARONSON "Decomposition of austenite by Diffusional Processes" edited by E. F. Zackay and H. I. Aaronson, (Wiley Interscience, New York, 1962) p. 387.
9. Y. OHMORI, A. T. DAVENPORT and R. W. K. HONEYCOMBE, *Trans. Iron Steel Inst. J.* **12**(1972) 129.
10. Y. OHMORI and R. W. K. HONEYCOMBE, *Trans. Iron Steel Inst. J.* **11** (1971) 1160.
11. H. I. AARONSON, Proceedings of the Phase Transformations Conference, Series 3 No. 11, Institute of Metallurgists, York, April 1979 Vol. 1 (Institute of Metallurgists, London, 1979) p. 11–1.
12. K. R. KINSMAN, E. EICHEN and H. I. AARONSON, *Met. Trans. A.* **6A** (1975) 303.
13. P. R. HOWELL, R. A. RICKS and R. W. K. HONEYCOMBE, *J. Mater. Sci.* **15** (1980) 376.
14. H. I. AARONSON and C. WELLS, *Trans. A. I. M. E.* (1956) 1216.
15. R. A. RICKS, G. S. BARRITTE and P. R. HOWELL, unpublished work.
16. K. C. RUSSELL and H. I. AARONSON, *J. Mater. Sci.* **10** (1975) 1991.
17. W. C. JOHNSON, C. L. WHITE, P. E. MARTH, P. K. RUF, S. M. TUOMINEN, K. D. WADE, K. C. RUSSELL and H. I. AARONSON, *Met. Trans. A.* **6A** (1975) 911.
18. R. G. BAKER and J. NUTTING, in "Precipitation processes in Steels" Iron and Steel Institute Special Report No 64, (Iron and Steel Institute, London, 1959, p. 1.
19. G. V. KURDJUMOV and G. SACHS, Z. PHYSIK **64** (1930) 325.
20. G. S. BARRITTE, R. A. RICKS and P. R. HOWELL, in "Quantitive Microanalysis with High Spatial Resolution" (The Metals Society, London) in press.
21. D. J. ABSON and R. E. DOLBY, Welding Institute Research Report No. 19/1978 (Welding Institute, London, 1978).
22. R. C. COCHRANE and P. R. KIRKWOOD, in "Trends in Steels and Consumables for Welding" Welding Institute Conference (The Welding Institute, Abingdon, 1978) p. 103.

Received 20 May
and accepted 24 July 1981